Pergamon

J. Mech. Phys. Solids, Vol. 42, No. 9, pp. 1375–1396, 1994

0022–5096/94 $7.00+0.00

0022–5096(94)E0031–X

BRITTLE FRACTURE UNDER A SLIDING LINE CONTACT

A. F. BOWER† and N. A. FLECK‡

†Division of Engineering, Brown University, Providence, RI 02906, U.S.A.; and
‡Cambridge University Engineering Department, Cambridge CB2 1PZ, U.K.

(*Received* 14 *October* 1993; *in revised form* 2 *April* 1994)

ABSTRACT

When an indenter slides over the surface of a brittle solid, cracks form in its wake. A simple analysis of this process is presented. The solid is modelled as an ideally brittle elastic half-space, which contains a distribution of short cracks near the surface, and is loaded by a cylindrical indenter. Two limiting cases of friction between the indenter and the half-space are considered. The cylinder may slide freely over the surface, with a fixed coefficient of friction between the contacting surfaces. Alternatively, the indenter may be perfectly bonded to the surface of the half-space. The loads necessary to cause fracture under the indenter are calculated, and compared to the loads required to initiate plastic deformation in the solid. In addition, the pattern of fracture which occurs under the indenter is analysed in detail. The residual tensile strength of a solid which has been damaged by contact loading is calculated. Finally, the influence of a residual stress near the surface of the half-space is investigated. It is shown that there is a critical tensile stress which leads to catastrophic failure under the indenter, while if the stresses are compressive, they may prevent fracture.

1. INTRODUCTION

Brittle solids such as ceramics and glasses are often used in applications where they are subjected to severe contact loading. Their high hardness and melting point makes them ideal wear resistant materials, so they are used in components such as bearings, seals and machine tools. In addition, ceramic components are frequently finished by grinding, which subjects the material near the surface to severe contact stresses. In all these cases, fracture of the material under the contact is a concern. Brittle fracture under service loading can be catastrophic, while small cracks introduced during grinding can significantly weaken a component (Lawn and Marshall, 1978; Marshall *et al.*, 1983).

There have been a number of experimental studies of brittle fracture under contact loading. A typical experiment involves pressing an indenter into the surface of the solid with a progressively increasing load, and observing the pattern of fracture which develops under the contact. Two types of indenter are generally used. The indenter may be "blunt", such as a sphere, or "sharp", such as a cone or Vickers pyramid. Depending on the geometry of the punch and the magnitude of the tractive load, a characteristic pattern of cracks forms under the contact. Under a blunt indenter, a well defined cone shaped crack "pops in" when the normal load reaches a critical

magnitude (Auerbach, 1891; Roesler, 1956; Chaudhri and Phillips, 1990). The mechanisms responsible for forming cone cracks are well understood. Since the stresses under a blunt indenter remain elastic up to the point of fracture, linear elastic fracture mechanics may be used to predict the conditions necessary to cause fracture. On this basis, a number of theoretical models have been developed which can predict both the fracture load and the subsequent length of the cracks (e.g. Frank and Lawn, 1967; Mouginot and Maugis, 1985).

Significant plastic deformation occurs under sharp indenters such as a cone or Vickers pyramid, so the pattern of fracture is more complicated. During normal loading, a penny shaped crack initiates at the tip of the indenter, and subsequently propagates radially to form a semi-circular crack perpendicular to the free surface. Several radial cracks of this type may form under pyramidal indenters. When the indenter is removed, a further penny-shaped crack forms almost parallel to the surface, driven by residual stresses. Cracks forming under a sharp indenter are difficult to analyse, because it is necessary to account for the plastic deformation under the contact. Models have been proposed which approximate the indentation process as a cavity expanding in an infinite solid (Lawn and Evans, 1977; Lawn *et al.*, 1980; Marshall and Lawn, 1979). These models have some limitations, but can predict qualitatively the shape and size of cracks forming under the contact.

The fracture pattern changes if the indenter slides over the surface under the action of a combined normal and tangential load. Under a blunt indenter, an array of cracks forms in the wake of the slider (Lawn, 1967; Bethune, 1976). The cracks are initiated at the trailing edge of the contact, and propagate almost perpendicular to the surface. In addition, there appears to be a characteristic spacing between neighboring cracks. The cracks which form under a sharp indenter are similar, but a crack with a plane perpendicular to the sliding direction also forms at the apex of the indenter (Veldkamp *et al.*, 1978; Swain, 1979).

Several simple models have been developed to predict the conditions necessary to cause fracture under a sliding indenter. For example, Lawn (1967), Bethune (1976), Swain (1979) and Veldkamp *et al.* (1979) have derived simple estimates of the fracture loads and the resulting crack sizes. More recently, Chen *et al.* (1991) have estimated stress intensity factors for cracks forming in the wake of a sharp indenter, by modelling a single semicircular flaw perpendicular to the free surface, and approximating the contact pressure distribution as a point force acting on the surface. Their predictions of the depth of the cracks were in good agreement with experimental measurements. Keer and Worden (1990) have calculated crack paths under rolling and sliding indentation. In addition, Keer and Kuo (1992) have calculated the spacing between cracks forming in the wake of a sliding point contact, by considering the behavior of two neighboring penny-shaped cracks in the wake of a sliding Hertzian pressure distribution. A detailed analysis of cracks forming under a blunt two-dimensional sliding contact has not so far been attempted, and is the subject of this paper.

To simplify the analysis, we have idealized the geometry using the two-dimensional model illustrated in Fig. 1. A half-space contains a distribution of small cracks, which initially have the same length c. The material is ideally brittle, with fracture toughness K_{IC}, and has elastic shear modulus G, Poisson's ratio ν and yield stress in tension σ_y. Since the stresses in the half-space are predominantly compressive, the faces of the

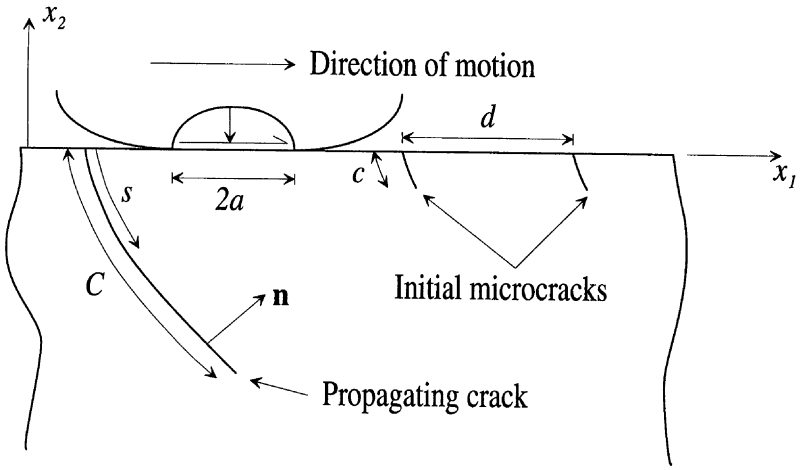

Fig. 1. A half-space containing several microcracks, loaded by a sliding Hertzian contact.

cracks may touch, and friction forces may act between them. Here, we model crack face friction using Coulomb's law, with a coefficient of friction μ_c. It is difficult to determine accurate values for crack face friction coefficients, but numerical tests have shown that the results we present here are not greatly affected by variations in μ_c. Unless otherwise stated, we have used a value of $\mu_c = 0.8$ in all our simulations.

The surface of the half-space is indented by a rigid cylinder. The normal contact pressure acting on the area of contact between the cylinder and the half-space is assumed to be Hertzian, given by

$$p = p_0\{1-(x-x_0)^2/a^2\}^{1/2}, \quad |x-x_0| < a, \tag{1.1}$$

where x_0 is the position of the center of the contact and p_0 is the peak Hertzian pressure.

Two limiting conditions of friction between the contacting surfaces have been considered. The cylinder may slide over the half-space, its motion being resisted by Coulomb friction. In this case, the surface of the half-space is subjected to a distribution of tangential traction

$$q = \pm\mu p_0\{1-(x-x_0)^2/a^2\}^{1/2}, \quad |x-x_0| < a. \tag{1.2}$$

The sign of the traction is such that the tractive force on the half-space acts in the direction of motion of the load. Alternatively, the cylinder may be perfectly bonded to the half-space. In this case, we assume that the cylinder is first pressed into the surface of the half-space, so that contact area is loaded by the distribution of pressure given in (1.1). Then, a steadily increasing tangential load Q is applied to the indenter. Since no slip occurs between the contacting surfaces, the contact area is subjected to tangential traction

$$q = \frac{Q}{\pi a}\{1-(x-x_0)^2/a^2\}^{-1/2}, \quad |x-x_0| < a. \tag{1.3}$$

If the contact stresses in the half-space are sufficiently high, the material near the surface fails by one of two mechanisms. In a material with low yield stress σ_y and

high toughness K_{IC}, the surface is plastically deformed. Alternatively, if the toughness is low and the yield stress high, the half-space fails by fracture. We begin by calculating the critical loads required to cause failure by both mechanisms. In addition, we investigate in detail the pattern of fracture which occurs in a brittle solid. For the case of a sliding indenter, it is shown that a periodic array of cracks forms in the wake of the slider, with an inclination almost perpendicular to the surface and a regular spacing between cracks. The depth and spacing of the cracks are calculated as a function of the applied loads. In contrast, if the indenter is perfectly bonded to the half-space, a single crack is initiated at the trailing edge of the contact when the tangential load reaches a critical magnitude. The crack continues to propagate if the tangential load is increased, and follows a trajectory that eventually returns to the free surface. Through this mechanism, a large wear particle is removed from the half-space.

We also calculate the residual strength of a solid damaged by contact loading. For this purpose, the shape and size of a series of cracks which form behind a sliding indenter are calculated. The contact load is then removed, and we calculate the magnitude of the critical tensile stress σ_{11} required to cause fracture in the damaged solid. Finally, we investigate the influence of residual stresses near the surface. It is shown that there is a critical level of tensile residual stress which causes catastrophic failure, while compressive stresses tend to prevent fracture.

Standard methods of linear elastic fracture mechanics have been used to analyse fracture in the half-space. The load induces mode I and mode II stress intensity factors K_I and K_{II} on each crack tip. A method for calculating K_I and K_{II} is summarized in Section 2.1. If K_I and K_{II} at a crack tip exceed a critical combination, the crack propagates. Here, we have used the intensity of the maximum tangential hoop stress as a mixed mode fracture criterion: the details of this procedure are described in Section 2.2. If the crack propagates, its path must be calculated. We have assumed that the path is such that the local mode II stress intensity factor at the crack tip vanishes during growth.

2. THEORY

We begin by describing a numerical procedure for analysing fracture under a sliding line contact. The problem to be solved is illustrated in Fig. 1: a half-space contains N cracks of length C_n, whose positions are specified by their parametric equations $\mathbf{z}(s)$, where s represents the arc length measured from one tip of the nth crack. Wherever a crack is pulled open by the load, its faces must be free of tractions. If the crack faces touch, friction forces may act between them: here, we assume that sliding between the crack faces is opposed by a traction $|\tau| \leqslant \mu_c|\sigma_n|$, where μ_c is the coefficient of crack face friction, and σ_n is the stress acting perpendicular to the crack. If the compressive stress acting on the crack faces is sufficiently large, parts of the crack lock up, so that the complete stress and displacement boundary conditions on the crack faces are given by

$$\left.\begin{aligned} |\tau_t| &\leqslant +\mu_c|\sigma_n|, \quad \dot{u}_t = 0 \quad \text{(locked)},\\ \tau_t &= +\mu_c|\sigma_n|, \quad \dot{u}_t > 0 \quad \text{(forward slip)},\\ \tau_t &= -\mu_c|\sigma_n|, \quad \dot{u}_t < 0 \quad \text{(reverse slip)}, \end{aligned}\right\} u_n = 0 \quad \text{(crack closed)} \tag{2.1}$$

$$\tau_t = \sigma_n = 0 \quad u_n > 0 \quad \text{(crack open)}, \tag{2.2}$$

where σ_n and τ_t are the normal and tangential tractions acting on the crack faces, u_n is the crack opening displacement and $\dot{u}_t$ denotes the rate of change of tangential displacement of the crack faces with time.

We seek to predict the behavior of the cracked half-space under the travelling load. The solution involves three stages:

(i) for a given position of the load, it is necessary to calculate the mode I and mode II stress intensity factors at each crack tip;
(ii) the stress intensity factors must then be compared with an appropriate fracture criterion;
(iii) if the criterion for fracture is exceeded, the cracks propagate, and the crack path needs to be calculated.

The steps in this process are described in turn below.

2.1. *Calculation of stress intensities*

A boundary integral formulation sometimes known as the "method of distributed dislocations" is the simplest way to calculate stress intensity factors in the cracked solid. This procedure was first applied to cracked solids subjected to contact loading by Keer and Bryant (1983) and by Bryant *et al.* (1984). The method has been described in detail elsewhere [see for example Nahrendran and Cleary (1984)], and so will only be briefly summarized here.

The solution begins by calculating the stresses induced by the load in the *uncracked* half-space, $\sigma'_{\alpha\beta}$. Expressions for $\sigma'_{\alpha\beta}$ induced by a sliding contact may be found in Johnson (1985), while those induced by a bonded contact may be found in Green and Zerna (1968). By adding a suitable distribution of dislocations along the line of each crack, these stresses are then corrected to satisfy the boundary conditions on the crack faces. Suppose that the stresses at a point $\mathbf{x}$ in the half-space due to a dislocation at $\mathbf{z}$ are given by $\sigma_{\alpha\beta} = \Lambda b_\gamma D_{\alpha\beta\gamma}(\mathbf{x}, \mathbf{z})$, where b_γ are the components of the Burgers vector, and $\Lambda = G/4\pi(1-\nu)$. Full expressions for D may be deduced from the complex potentials given in Bryant *et al.* (1984). The combined stresses at $\mathbf{x}$ due to the contact load and distributions of dislocations along each crack are then

$$\sigma_{\alpha\beta}(\mathbf{x}) = \sigma'_{\alpha\beta}(\mathbf{x}) + \sum_{n=1}^{N} \int_0^{C_n} b_\gamma(s)\Lambda D_{\alpha\beta\gamma}[\mathbf{x}, \mathbf{z}(s)]\, \mathrm{d}s. \tag{2.3}$$

In (2.3) and elsewhere, we use the convention that Greek subscripts range from 1 to 2, and a repeated suffix denotes summation. In particular, the tractions τ_α at a point η on the faces of the mth crack are

$$\tau_\alpha = n_\beta(\eta)\left\{\sigma'_{\alpha\beta}(\mathbf{z}(\eta)) + \sum_{n=1}^{N}\int_0^{C_n} b_\gamma(s)\Lambda G_{\alpha\beta\gamma}[\mathbf{z}(\eta), \mathbf{z}(s)]\,\mathrm{d}s\right\}, \tag{2.4}$$

where $n_\alpha(\eta)$ are the components of a unit vector normal to the plane of the crack at η, as shown in Fig. 1. The integrands in (2.3) and (2.4) may be shown to tend to $(s-\eta)^{-1}$ as $s \to \eta$. Consequently, for $n = m$, we take Cauchy principal values of the integrals in (2.4). The displacement of the faces of the crack at η is related to the dislocation distribution by

$$u_\alpha(\eta) = -\int_{C_n}^{\eta} b_\alpha(s)\,\mathrm{d}s. \tag{2.5}$$

Along any subsurface cracks, the dislocation distribution must satisfy the closure constraint

$$\int_0^{C_m} b_\alpha(s)\,\mathrm{d}s = 0. \tag{2.6}$$

Substituting equations (2.3)–(2.5) into the boundary conditions listed in (2.1) and (2.2) leads to a set of coupled integral equations for the unknown dislocation densities, which may be solved using standard numerical methods [see for example Erdogan and Gupta (1972) and Gerasoulis (1980)]. In our solution we used a piecewise-linear scheme similar to that developed by Gerasoulis (1980). When interpolating the dislocation density, we assumed that the distribution was bounded at the crack mouth and square-root singular at the tip.

The solution is complicated by the fact that the positions of open, closed, locked and slipping zones in the cracks are not known *a priori*, and must be determined as part of the solution. In addition, (2.2) shows that unless the crack is fully open or $\mu_c = 0$, the solution depends on the history of loading. The distribution of dislocations must therefore be updated progressively as the load moves over the surface of the half-space. Here, we have used a simple time stepping scheme to approximate the history of loading. The load is moved over the surface in a series of steps, and a solution is found for successive positions of the load. The time derivative of b_α is estimated as $\dot{b}_\alpha(\hat{s}, T) = (b_\alpha(\hat{s}, T+\Delta T) - b_\alpha(\hat{s}, T))/\Delta T$, where $b_\alpha(\hat{s}, T+\Delta T)$ and $b_\alpha(\hat{s}, T)$ represent the values of b at the current and preceding load steps. The positions of open, closed, locked and slipping regions in the crack are found using an iterative procedure. The calculation begins with a suitable initial guess for the configuration of the crack, and a solution is found for $b_\alpha(\hat{s}, T+\Delta T)$. A new approximation to the crack configuration is found by checking the traction and displacement boundary conditions on the crack faces. The crack is assumed to close wherever the crack faces overlap, while the crack is opened at points where tensile stresses are found. Similarly, locked zones are checked to see whether $|\tau| < |\sigma_n|$. If this condition is violated, the crack faces are allowed to slip. Finally, the sliping regions are checked to ensure that the friction force opposes the direction of motion of the crack faces. The crack is locked at any point where this is not the case. Once a new configuration of the crack

has been found, a corrected solution for b_α is calculated, and the process is repeated until the solution converges.

Once a solution for b_α has been found, stress intensity factors may be extracted from the dislocation distribution by considering the asymptotic form of the crack opening displacement at each crack tip, with the result

$$K_{\mathrm{I}} = 2\pi\sqrt{\pi\Lambda}\lim_{s\to C_n}\sqrt{(C_n-s)}\,b_\alpha(s)n_\alpha(s),$$

$$K_{\mathrm{II}} = 2\pi\sqrt{\pi\Lambda}\lim_{s\to C_n}\sqrt{(C_n-s)}\,b_\alpha(s)t_\alpha(s). \tag{2.7}$$

2.2. *Fracture criterion*

If K_{I} and K_{II} exceed some critical combination, the crack will start to propagate. Here, we use the intensity of the greatest tensile hoop stress as a mixed-mode fracture criterion. The maximum principal stresses at a crack tip occur at an angle

$$\theta_0 = \frac{3K_{\mathrm{II}}^2 \pm K_{\mathrm{I}}(8K_{\mathrm{II}}^2+K_{\mathrm{I}}^2)^{1/2}}{9K_{\mathrm{II}}^2+K_{\mathrm{I}}^2} \tag{2.8}$$

and have an intensity

$$K_\sigma = \cos\frac{\theta_0}{2}\left\{K_{\mathrm{I}}\cos^2\frac{\theta_0}{2} - \frac{3}{2}K_{\mathrm{II}}\sin\theta_0\right\}. \tag{2.9}$$

According to the maximum hoop stress criterion, a crack under mixed-mode loading starts to propagate when $K_\sigma \geqslant K_{\mathrm{IC}}$, and forms a kink at an angle θ_0. In fact, the results presented here are not sensitive to the choice of a criterion for mixed mode fracture. Even ignoring the effects of K_{II} altogether, so that the crack is assumed to advance when $K_{\mathrm{I}} > K_{\mathrm{IC}}$, produces little change in the results.

Once a crack starts to propagate, its direction of growth must be calculated. Here, we have assumed that the cracks follow a path such that $K_{\mathrm{II}} = 0$ at the local crack tip. For simplicity, the crack path was assumed to be smooth, so the cracks may curve but not kink. In practice, the crack may kink when it first begins to propagate, but numerical tests have shown that the predicted crack shape is not significantly changed when crack kinking is taken into account.

For numerical purposes, the geometry of each crack was approximated by a series of segments with piecewise constant curvature. To extend a crack, an additional segment was added to the crack tip. Using an iterative method, the curvature of the new segment was chosen to satisfy the $K_{\mathrm{II}} = 0$ fracture criterion.

3. RESULTS AND DISCUSSION

Consider the problem illustrated in Fig. 1. A brittle half-space contains a distribution of microcracks, and is subjected to contact loading. Our objective is to calculate the critical loads required to cause the solid to fail, and to investigate in

detail the nature of the mechanism of failure. Two limiting conditions of friction between the indenter and the half-space are considered in our analysis. The indenter may either slide over the surface of the half-space, with Coulomb friction acting between the contacting surfaces. Alternatively, the indenter may be perfectly bonded to the surface of the half-space. It is convenient to discuss the two cases separately.

3.1. *Fracture under a sliding contact*

Before attempting a full scale numerical simulation of the behavior of the cracked half-space under contact loading, we may make some approximate predictions by examining the nature of the stress field under a sliding Hertzian contact. Fracture is most likely to initiate in the region of the half-space which is subjected to the greatest tensile stress. It is straightforward to show that the tensile stress is greatest at the surface, immediately behind the contact. In this region, the variation of stress with depth is given approximately by

$$\sigma_{11} \approx \mu p_0\left(2-\frac{5}{2}\sqrt{\frac{z}{a}}\right)-p_0\frac{3}{2}\sqrt{\frac{z}{a}}+2\frac{z}{a}, \quad \sigma_{22}=\sigma_{12}=0, \tag{3.1}$$

where p_0 is the peak Hertzian pressure and a is half the width of the contact, as defined in (1.1) and (1.2). Now, assume that the half-space contains a large number of microcracks, with lengths c, distributed randomly through the solid. Clearly, fracture is most likely to initiate at a surface breaking crack which is perpendicular to the free surface, located at the trailing edge of the contact. The stress intensity factors for such a crack may be estimated as $K_{\mathrm{I}} \approx 1.12\sigma\sqrt{\pi c}$, $K_{\mathrm{II}} \approx 0$, where σ is the stress acting half-way down the crack, calculated using (3.1). Thus

$$K_{\mathrm{I}} \approx 1.12\left[\mu p_0\left(2-\frac{5}{2}\sqrt{\frac{c}{2a}}\right)-p_0\left(\frac{3}{2}\sqrt{\frac{c}{2a}}-\frac{c}{a}\right)\right]\sqrt{\pi c}. \tag{3.2}$$

The critical load required to initiate fracture in the half-space, p_0^{fract} is reached when $K_{\mathrm{I}} = K_{\mathrm{IC}}$, giving

$$p_0^{\mathrm{fract}} = \frac{K_{\mathrm{IC}}}{1.121\sqrt{\pi c}\{\mu(2-2.5\sqrt{c/2a})-1.5\sqrt{c/2a}+c/a\}} \tag{3.3}$$

The accuracy of this estimate may be confirmed by numerical calculations, as follows. Figure 2 shows the variation of stress intensity factors for a single surface breaking microcrack, with orientation perpendicular to the free surface, as the load moves over the half-space. Results are shown for various microcrack lengths, and for two values of the surface traction coefficient. As expected, the maximum value of K_{I} occurs when the crack is at the trailing edge of the contact, at which point K_{II} is small. Indeed, the mode II stress intensities are small throughout the cycle of load, due to friction between the crack faces. The fracture load predicted by (3.3) is plotted on Fig. 3, together with the more accurate numerical predictions. It is evident that, provided the initial crack length is small compared to the contact width ($c/a < 0.1$), the approximate result is very accurate.

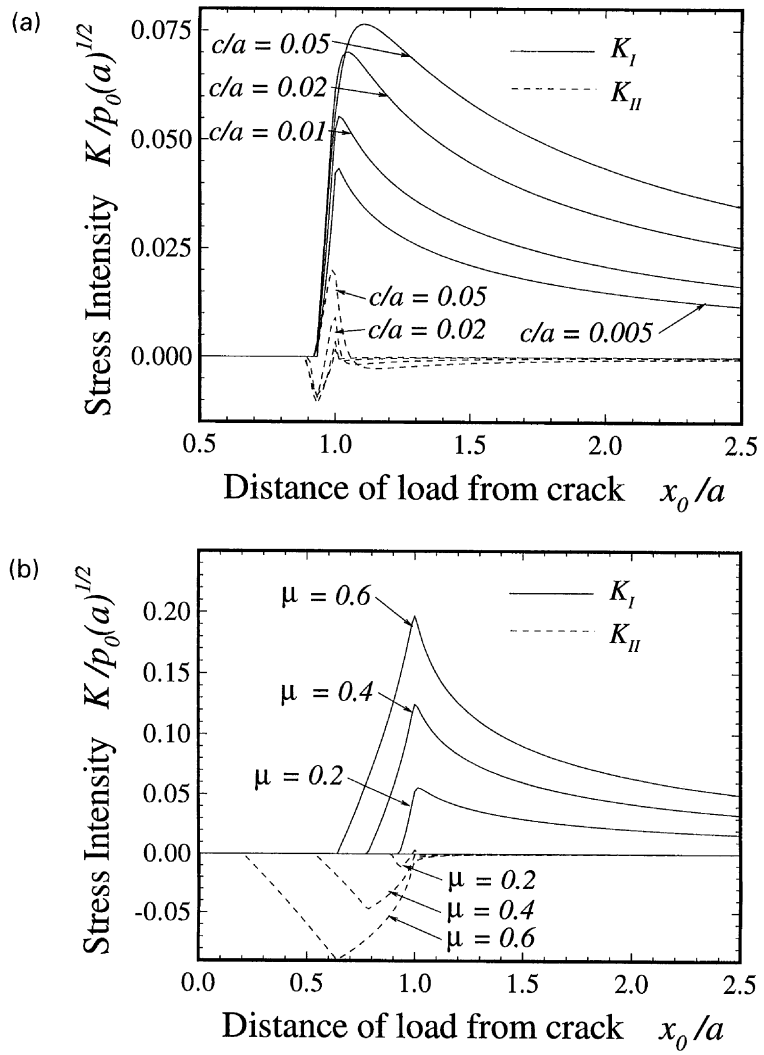

Fig. 2. The stress intensity factors at the tip of a vertical surface breaking microcrack, as a function of the distance of the load from the crack mouth. Crack face friction coeff. $\mu_c = 0.8$; (a) traction coeff. $\mu = 0.2$; (b) crack length $c/a = 0.01$.

If the initial crack size is very small compared to the contact width, then (3.3) may be simplified further to:

$$p_0^{\text{fract}} \approx 1.26 \frac{K_{\text{IC}}}{\mu\sqrt{c}}. \tag{3.4}$$

The fracture load may be compared with the load required to cause plastic flow in the half-space. The loads required to cause repeated plastic deformation have been calculated by Bower and Johnson (1989), and are given by

$$p_0^{\text{def}} = \begin{cases} \sigma_y/\mu\sqrt{3}, & \mu > 0.25 \\ 4\sigma_y/\sqrt{3}, & \mu < 0.25. \end{cases} \tag{3.5}$$

If $p_0^{\text{def}} > p_0^{\text{fract}}$, the material is more likely to fail by fracture than plastic flow. For $\mu > 0.25$, the mechanism of failure is determined by the properties of the material

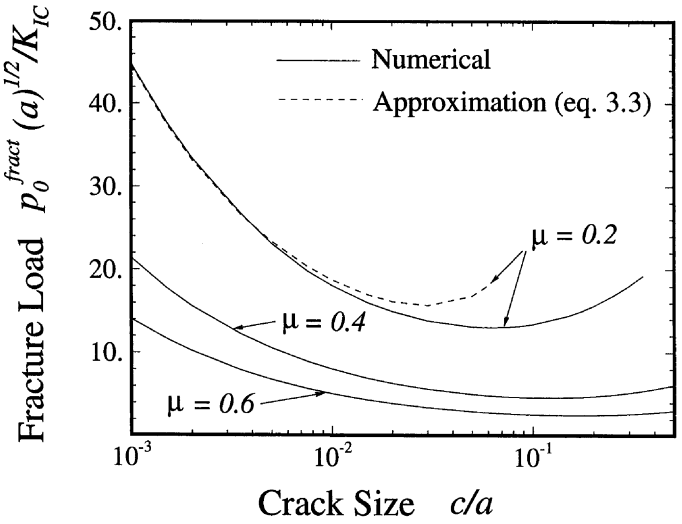

Fig. 3. The peak Hertzian pressure required to initiate fracture in a half-space which contains surface breaking microcracks, as a function of microcrack length c/a and surface traction coefficient μ.

and the initial flaw size c, and is independent of loading. We may define a material parameter Φ which determines the mechanism of failure as follows:

$$\Phi = \frac{p_0^{\text{fract}}}{p_0^{\text{def}}} \approx 2.18 \frac{K_{\text{IC}}}{\sigma_y \sqrt{c}} \approx 0.73 \frac{K_{\text{IC}}}{H\sqrt{c}}, \tag{3.6}$$

where H is the hardness of the solid. For $\Phi < 1$, a solid will fail by fracture, while for $\Phi > 1$, it will fail by plastic deformation. Approximate values of Φ for various classes of material are displayed in Table 1, where the initial flaw size c has been taken as 10 μm. It is evident that only the most brittle and hard materials such as ceramics and glasses are likely to fracture without plasticity. Polymers have Φ close to 1, and may

Table 1. *Estimated values of fracture parameter* Φ *for various materials. For* $\Phi < 1$ *the material fractures; for* $\Phi > 1$ *it yields*

Material	σ_y (MNm^{-2})	K_{IC} (MNm$^{-3/2}$)	Φ
SiC; Si_3N_4	10,000	3–8	0.1–0.3
Soda glass	4000	0.7	0.13
Silica glass	7000	2–3	0.15–0.2
Alumina	5000	3–5	0.2–0.5
Ice	85	0.15	1.2
Epoxy	30–100	0.3–0.4	2–8
Ball bearing steels	3000	20	5
PMMA	60–100	0.9–1.4	7–12
Nylons	50–80	2.5	20–30
Co/WC cermets	400–900	14–16	11–29
Pressure vessel steel	1700	170	72
Carbon steels	300–1500	50–150	24–370
Aluminium alloys	100–600	23–45	28–330

fail by a combination of fracture and plastic deformation. For even the most brittle steels, plastic flow is the probable mechanism of failure. If the traction coefficient is less than 0.25, fracture becomes progressively less likely.

We proceed to investigate the process of fracture under the sliding contact in more detail. Suppose that the half-space contains a single microcrack, which meets the surface at a right angle, and that the contact pressure exceeds the fracture load. At some point during the passage of the load over the crack, the crack tip stress intensity factor reaches the fracture toughness of the solid, and the crack starts to propagate. Qualitatively, its subsequent behavior may be deduced using (3.2). For $c/a \ll 1$, $K_I \approx 2.2\mu p_0\sqrt{\pi c}$, so K_I initially increases with crack length. The crack is therefore unstable: as the crack length increases, the stress intensity factor increases beyond the fracture toughness, tending to increase the rate of propagation. However, the tensile stress decays very rapidly below the surface of the half-space, so K_I quickly reaches a maximum and begins to decay. The crack continues to propagate until the value of K_I drops to K_{IC}, at which point it arrests.

The numerical results presented in Fig. 4 illustrate this behavior. The figure shows the predicted sequence of crack shapes as the load passes over the surface, for a relatively high surface traction coefficient ($\mu = 0.4$), assuming that the load exceeds the fracture load by 20%. Although Fig. 4 shows results for three neighboring microcracks at the surface of the half-space, the behavior of the first crack to pass under the load is indistinguishable from that of an isolated crack in the solid. When the load reaches $x_0/a \approx 0.9$, the crack jumps instantly to a new length, with no change in the position of the load. Subsequently, some further stable crack growth occurs: the crack stops propagating once the load is some distance away.

Figure 4 shows that the final length of the fracture is almost an order of magnitude greater than the initial length of the microcrack. There is an important consequence of this result. The shape and size of the fractures forming in the wake of a slider are

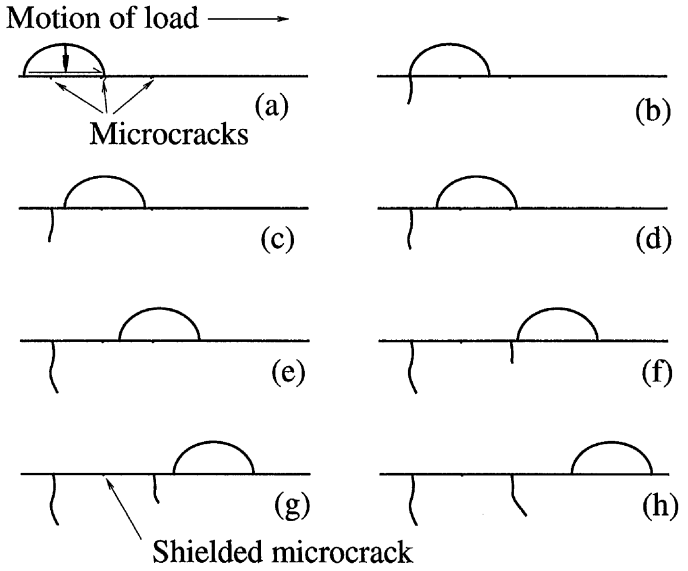

Fig. 4. The behavior of three microcracks at the surface as the load passes over them. Parameters: crack length $c/a = 0.025$, load $p_0/p_0^{\text{fract}} = 1.2$, friction coeff. $\mu = 0.4$, crack face friction coefficient $f = 0.8$; distance between microcracks $d/a = 1.25$.

determined by the contact geometry, and are not sensitive to the configuration of the microcrack responsible for the failure. The main role of the initial microcrack size c is to determine the fracture load p_0^{fract}.

Experimental observations of fracture behind a sliding contact have shown that a periodic array of cracks forms in the wake of the indenter, with a characteristic spacing between the cracks. It is not difficult to explain this behavior. Suppose that there are two microcracks at the surface of the half-space, with only a small distance between them. The first crack to pass under the load becomes unstable before the second, and jumps instantly to a depth which greatly exceeds its initial length. The stress field under the indenter is significantly altered by the presence of this crack, and while the slider is close to the crack, the tensile stresses in its wake are substantially reduced. If the second microcrack is close to the first, it is unlikely to propagate.

Figure 4 demonstrates the effects of this interaction between cracks. There are three neighboring microcracks at the surface of the half-space: the first crack to pass under the load propagates, but its neighbor is shielded and remains stable. By the time the load reaches the third crack, the stress field under the indenter is no longer significantly affected by the first fracture. The third microcrack therefore propagates in a similar manner to the first.

If the spacing between microcracks is much less than the contact width, then the distance between successive fractures is determined by this shielding effect. We have used the following approach to estimate the critical spacing between fractures. First, we calculate the shape of a single fracture initiated from a microcrack of length c in the wake of the indenter. The load is then progressively moved past the first crack. At each step, stress intensity factors are calculated for a second microcrack, also of length c, located at the trailing edge of the contact. The stress intensities for the second microcrack are found to increase at the load moves away from the first fracture: the critical spacing is taken to be the point where the stress intensity just reaches the fracture toughness of the solid. The predicted spacing is shown in Fig. 5, as a function of the load factor p_0/p_0^{fract} and friction coefficient μ. For high values of p_0/p_0^{fract}, the

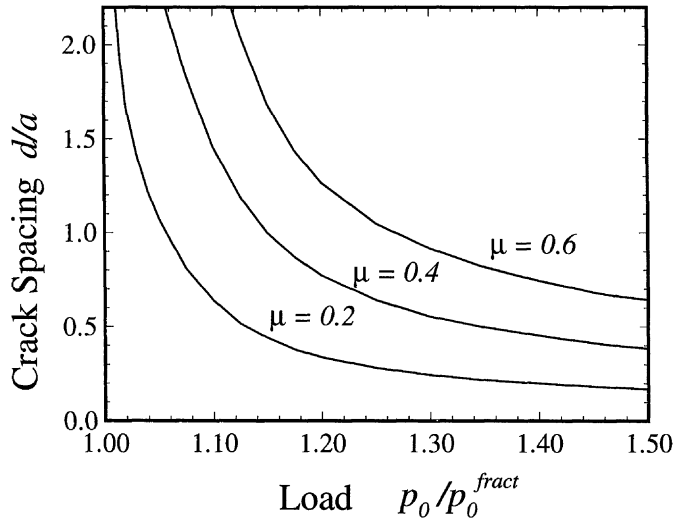

Fig. 5. Critical spacing between fractures forming in the wake of a sliding contact, as a function of the peak Hertzian load and traction coefficient.

spacing appears to approach an asymptotic value. Our results are in good qualitative agreement with experimental observations reported by Veldkamp *et al.* (1978). Our predictions are also similar to those of Keer and Kuo (1992), who used a more sophisticated three-dimensional model to calculate the crack spacing. We have also investigated the influence of the initial flaw size, but have found that its main influence is to set the value of p_0^{fract}. For a given value of p_0/p_0^{fract}, the microcrack size does not appear to have much effect on the crack spacing.

The simulation shown on Fig. 4 shows that interaction between neighboring cracks has some influence on their shape. The middle microcrack of Fig. 4 does not propagate under the contact loading and will be neglected in the following discussion. The left-most microcrack grows first and the crack on the right grows second. The second fracture only propagates to approximately 4/5 the depth of the first, and its shape is also significantly different. However, numerical tests show that the behavior of a third fracture is very similar to that of the second, suggesting that a crack only interacts significantly with its nearest neighbor. We have therefore taken the shape of the second crack to be indicative of the steady-state crack shape. On this basis, a set of steady state crack shapes for various initial flaw sizes, magnitudes of load, and coefficients of friction has been plotted in Fig. 6. Qualitatively, the shape of the cracks is similar for each case. Unless the coefficient of friction is particularly large ($\mu > 0.6$), the cracks propagate roughly perpendicular to the free surface. The depth of the cracks increases rapidly with load or friction coefficient, and is also sensitive to the initial flaw size.

In principle, the fracture process we have described may be the basis of a mechanism of wear. One might expect that successive fractures forming in the wake of the slider would coalesce, and generate a wear particle. However, we have not observed this effect in any of our simulations. If the load passes over the half-space only once, then the separation between the cracks forming in its wake is always too large for the cracks to coalesce, even under extremely high loads. The separation between cracks may be reduced if the first pass of the load is followed by another, with a different magnitude; contact width; or friction coefficient. An example is shown in Fig. 7, which shows the behavior of four neighboring microcracks under two successive passes of the load, at a fixed contact width. Figure 7(a) shows the pattern of fracture which develops after the first passage of the load; Fig. 7(b) shows the pattern after the second load. The first load has magnitude $p_0/p_0^{\text{fract}} = 1.125$ and friction coefficient $\mu = 0.6$. The separation between the microcracks is such that only the first and third cracks propagate; the second and fourth are shielded by their neighbors. The second load has magnitude $p_0/p_0^{\text{fract}} = 1.75$ and friction coefficient $\mu = 0.2$. This load is sufficient to cause the remaining microcracks to propagate. However, they are deflected away from their neighbors and do not coalesce with them. We have observed a similar effect if the direction of motion of the load over the half-space is reversed, so that the solid is subjected to two successive contacts travelling in opposite directions. This behavior is not difficult to explain: the material surrounding each crack is shielded from stress, and it is not easy for a second crack to propagate through the unloaded region.

To some extent, our observation that neighboring cracks do not coalesce is a consequence of the two-dimensional nature of our model. The three-dimensional

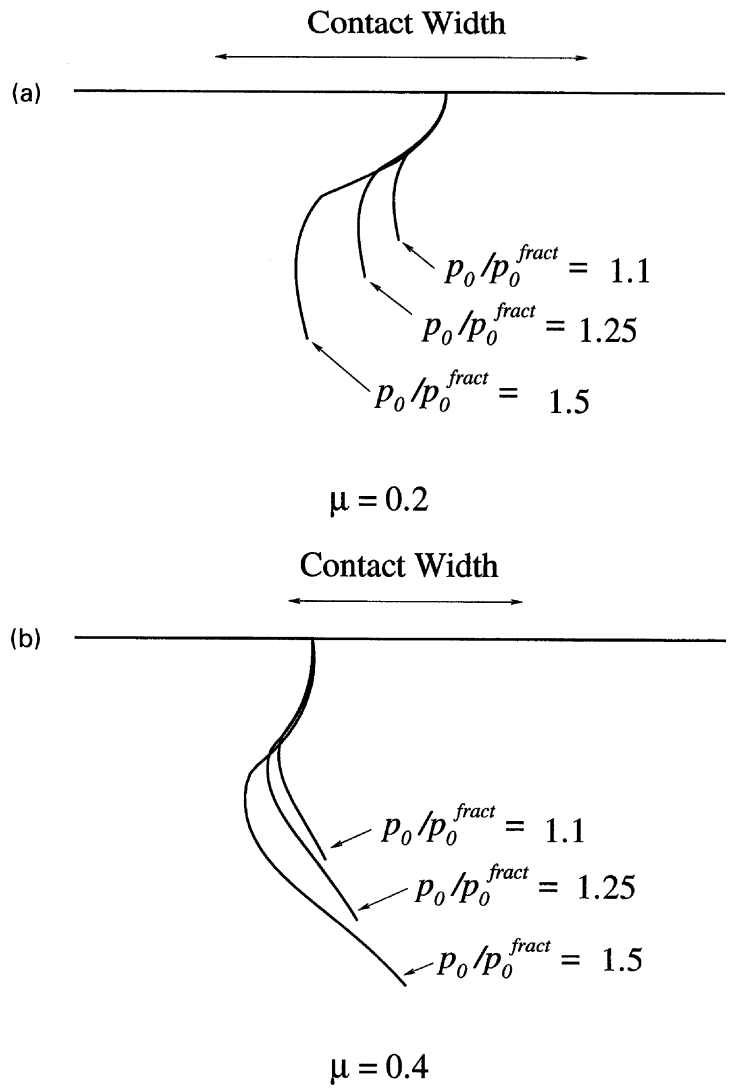

Fig. 6. Steady state profiles of cracks forming under a sliding line contact. (a) $\mu = 0.2$, $c/a = 0.01$; (b) $\mu = 0.4$, $c/a = 0.01$; (c) $\mu = 0.6$, $c/a = 0.01$; (d) $p_0/p_0^{\text{fract}} = 1.2$, $\mu = 0.4$.

cracks which form under a point contact are likely to interact less strongly than the edge cracks produced by a line contact. In addition, cracks which run parallel to the surface may be initiated by point contacts. Such cracks would almost certainly coalesce with the edge cracks we have described here, and would produce wear debris. However, our observations suggest that, although fracture under sliding contacts severely damages a surface, the rate at which material is removed from the solid due to fracture is likely to be relatively slow.

3.2. *Fracture under a bonded line contact*

In the preceding section, we considered the damage caused by an indenter which slides freely over the surface of the half-space. We proceed to investigate the failure process under a perfectly bonded indenter.

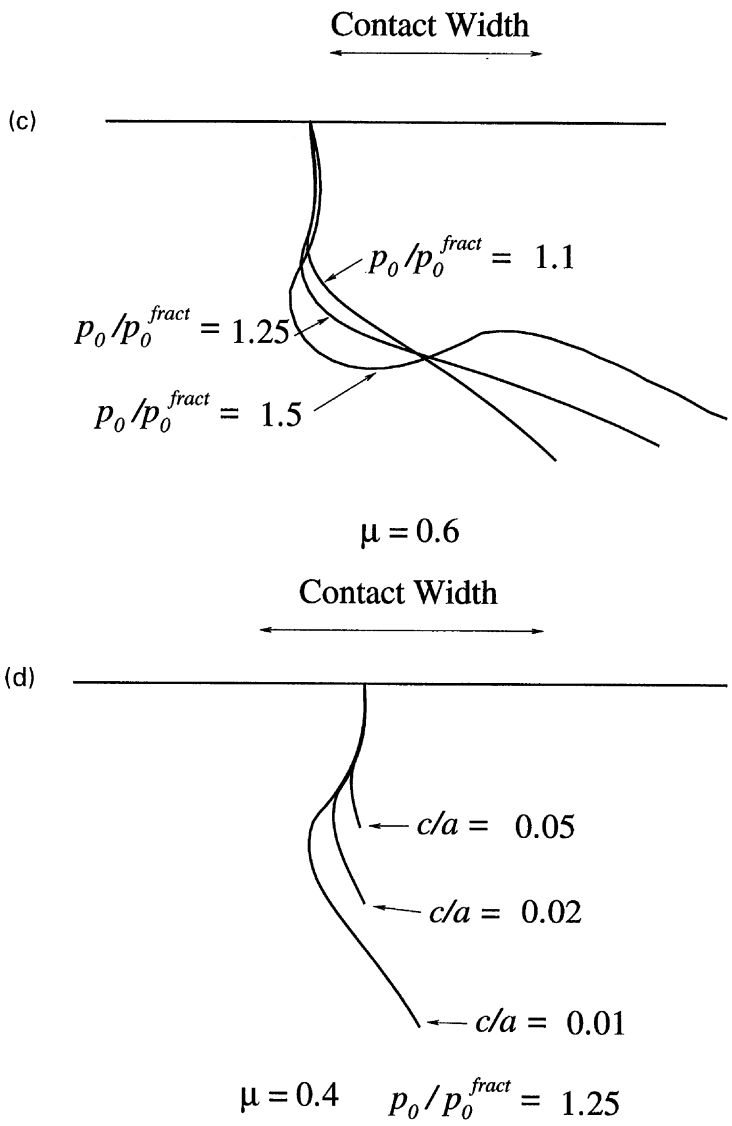

Fig. 6 (*continued*).

We assume that the half-space is loaded in the following manner. First, a rigid cylinder is pressed into its surface by a normal load, magnitude P per unit length. This subjects the half-space to the Hertzian distribution of pressure given in (1.1), with $p_0 = 2p/\pi a$. Subsequently, with P held constant, a progressively increasing tangential traction Q is applied to the indenter. It is assumed that no slip occurs in the interface between the cylinder and half-space, so that the distribution of tangential traction given in (1.3) acts on the area of contact.

The tangential load induces a singular distribution of stress at the edges of the contact area. The normal load does not induce stresses in this region and so does not play a role in initiating fracture. The distribution of stress near the edge of the contact is identical to the asymptotic field at the tip of a mode II crack. One may define a corresponding stress intensity factor, which is related to the applied load by

$$K_{II} = Q/\sqrt{\pi a}. \tag{3.7}$$

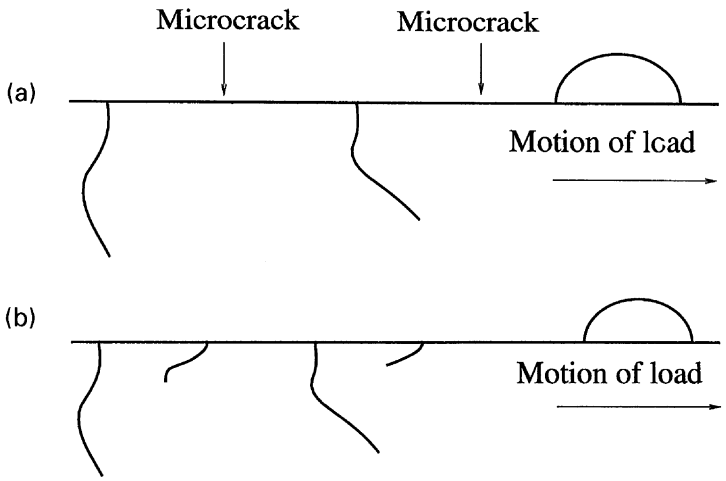

Fig. 7. The pattern of fracture which develops under two successive passes of the load. (a) Cracks which form under the first load; magnitude $p_0/p_0^{\text{fract}} = 1.125$, $\mu = 0.6$. (b) The fracture pattern after the second load; magnitude $p_0/p_0^{\text{fract}} = 1.75$, $\mu = 0.2$.

Therefore, in an ideally brittle solid, fracture will initiate spontaneously at the edge of the contact when the tangential load reaches a critical value, irrespective of the distribution of microcracks in the solid. If one uses the maximum hoop stress intensity factor as a mixed mode fracture criterion, the critical load is given by

$$Q^{\text{fract}} = 0.866 K_{\text{IC}} \sqrt{\pi a}. \tag{3.8}$$

The same criterion predicts that a crack will initiate at the trailing edge of the contact, at an angle of 70.5° to the surface.

The subsequent path of the crack depends on the magnitude of the normal load P acting on the cylinder. In Fig. 8, we have plotted the crack paths for various values of P/Q^{fract}. For small values of $P/Q^{\text{fract}} < 0.2$ the crack propagates unstably (i.e. under constant applied load), and follows a trajectory which gradually curves up towards

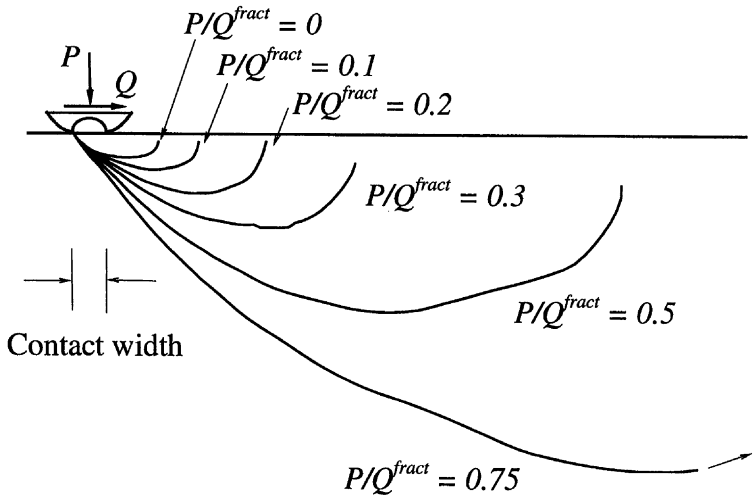

Fig. 8. Crack paths under a bonded line contact.

the surface. As the crack approaches the free surface on the far side of the contact, it eventually reaches a region where the stress field is compressive and arrests. For larger values of P/Q^{fract}, the crack propagates unstably for a short distance, then arrests. If the magnitude of the tangential load is increased beyond Q_{fract}, the crack continues to propagate, and progressively turns up towards the surface. Eventually, it reaches a zone of high compressive stress near the free surface and arrests. Figure 8 shows the configuration of the crack after it arrests, for several values of P/Q^{fract}. Increasing the magnitude of the tangential load does not cause the crack to propagate beyond this point. However, the ligament of material between the crack tip and the free surface is very weak. For example, if a small tensile load is applied to the indenter, one finds that the crack runs up to the free surface. Consequently, the material between the crack and the free surface would almost certainly be removed as a wear particle. If the magnitude of the normal load P is increased, the compressive stress field below the indenter tends to drive the crack deeper into the half-space. However, the crack always eventually curves back towards the free surface before it eventually arrests.

These results suggest that if seizure occurs between the contacting surfaces, the wear rate by fracture is likely to be catastrophic. Figure 8 shows that, even for small values of P/Q^{fract}, the size of the wear particle is several times greater than the width of the contact.

3.3. *Residual strength of a damaged half-space*

We conclude by investigating the influence of tensile stresses, which act parallel to the surface of the half-space, on the failure of the solid. First, we calculate the residual strength of a half-space which has been damaged by contact loading. For this purpose, we suppose that the half-space is first loaded by a sliding cylinder, as described in Section 3.1. The contact loading initiates an array of edge cracks at the surface of the solid. The contact load is then removed, and the half-space is subjected to a remote tensile stress σ_{11} acting parallel to the surface. There is a critical magnitude of remote stress which causes the cracks induced by the contact load to propagate, and results in catastrophic failure of the solid.

We have calculated the critical remote stress as a function of the contact loads applied to the solid and the initial crack size. To calculate the residual strength, we assumed that the half-space contained three neighboring microcracks, separated by a distance $d/a = 2$. We calculated the final shape of each crack after the load had traversed the surface of the half-space. We then found the level of residual stress required to cause one of the cracks to continue to propagate in the absence of the contact. The results of our calculations are displayed in Fig. 9. The residual strength is specified as the ratio of stress required to cause fracture to the Hertzian fracture load, $\sigma_{11}/p_0^{\text{fract}}$, where p_0^{fract} is given in (3.3). It is shown as a function of the load factor p_0/p_0^{fract} for various values of friction coefficient μ in Fig. 9(a), and as a function of initial microcrack lengths c/a in Fig. 9(b). For comparison, one may calculate the stress required to cause fracture in a solid which has not been damaged by contact loading, and contains only the initial microcracks. The fracture stress is given by

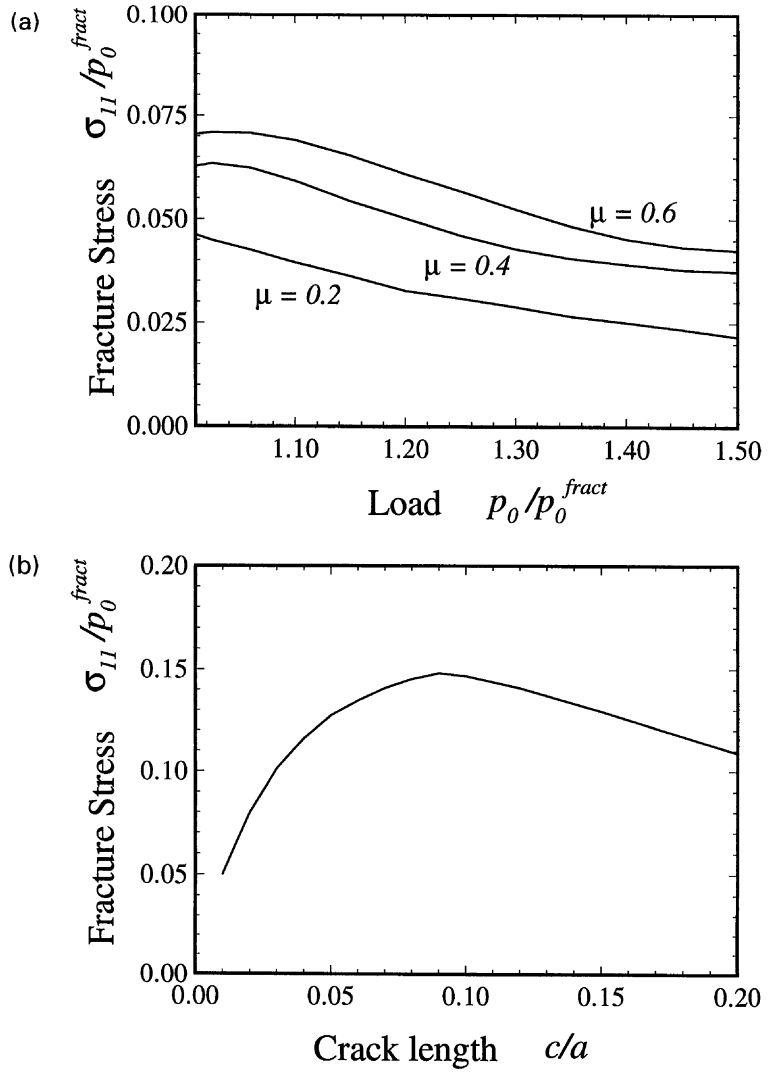

Fig. 9. The residual strength of a half-space damaged by contact loading. (a) Variation with contact loads, for microcrack size $c/a = 0.01$; (b) variation with crack size, for contact loads $p_0/p_0^{\text{fract}} = 1.2$, $\mu = 0.4$.

$$\sigma_{11} = \frac{K_{IC}}{1.121\sqrt{\pi c}}, \tag{3.9}$$

so that from (3.3),

$$\frac{\sigma_{11}}{p_0^{\text{fract}}} = \mu(2-2.5\sqrt{c/2a}) - 1.5\sqrt{c/2a} + c/a. \tag{3.10}$$

It is evident that the damage caused by contact loading reduces the strength of the solid by almost an order of magnitude.

3.4. *The influence of near-surface residual stresses*

We have also calculated the level of residual stress which, when applied together with the contact loading, causes catastrophic fracture in the half-space. This is some-

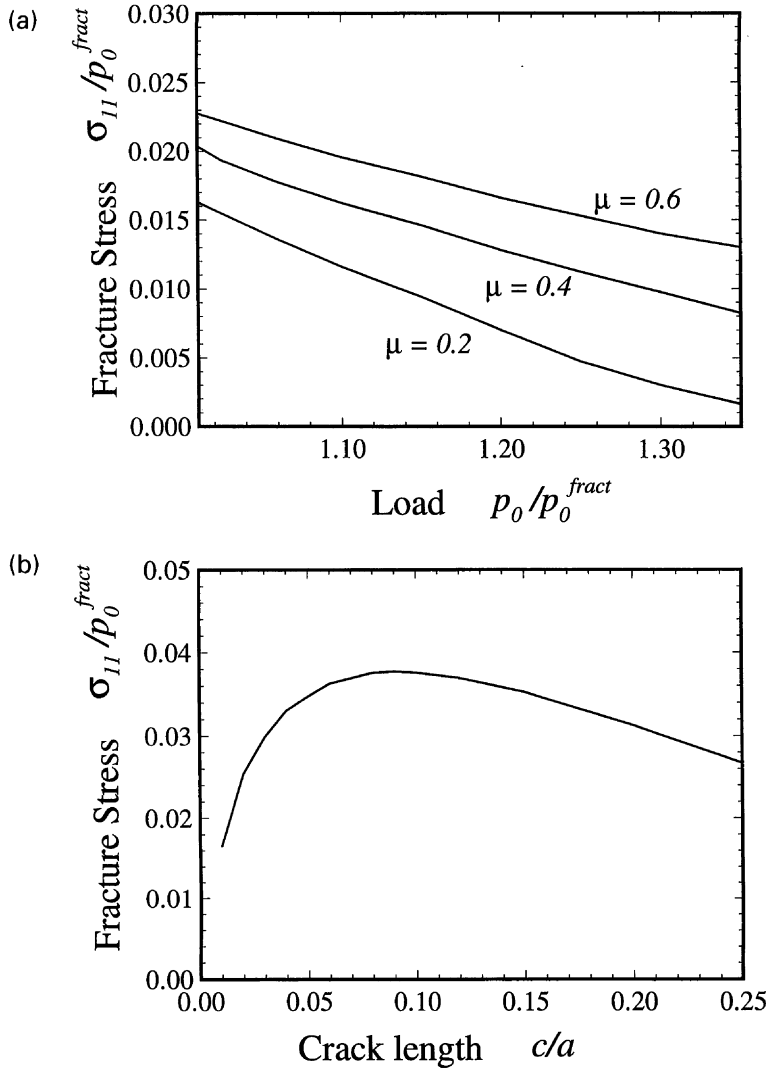

Fig. 10. The residual stress required to cause catastrophic fracture in a solid subjected to contact loads. (a) Variation with contact loads, for microcrack size $c/a = 0.01$; (b) variation with crack size, for contact loads $p_0/p_0^{fract} = 1.2$, $\mu = 0.4$.

what less than the residual strength of the solid, since the contact and residual stresses act in a co-operative manner at the point where unstable fracture occurs. In addition, the path of the cracks is influenced by the residual stress.

We used an iterative technique to calculate the critical stress. For simplicity, we assumed that the half-space contained only one initial microcrack at its surface. The residual stress is taken to be uniform, and to act in a direction parallel to the free surface. With an appropriate initial guess for the magnitude of the residual stress, the contact load was applied to the half-space. Depending on whether unstable fracture was found to occur, the residual stress was modified appropriately. This procedure was repeated until successive approximations to the residual stress differed by less than 1%. The results are shown in Fig. 10, which shows the critical residual stress as a function of the applied loads and the initial crack length. It appears that the magnitude of the residual stress required to cause catastrophic failure under inden-

tation loading is only a fraction of the stress required to fracture the solid in the absence of contact loading.

4. CONCLUSIONS

We have described a detailed analysis of the damage caused by a cylinder sliding over the surface of a brittle solid. Two limiting cases of friction between the contacting surfaces were considered: the cylinder was either assumed to slide over the surface, with Coulomb friction acting in the interface; or else was assumed to bond perfectly to the mating surface.

For a sliding indenter, it was shown that the critical loads required to cause fracture may be estimated using a simple closed-form expression given in (3.3). The loads required to initiate fracture were compared to those needed to cause the material to deform plastically. It was shown that only extremely brittle materials such as ceramics and glasses are likely to fail by brittle fracture under contact loading. Polymers may fail by a mechanism of combined plastic flow and fracture. In other materials, failure will almost certainly be by plastic flow at the surface.

The pattern of fracture caused by a sliding contact was also investigated. It was shown that the shape and size of the cracks which form in the wake of the slider are determined by the geometry of the contact and the load ratio p_0/p_0^{fract}, and are relatively insensitive to the initial flaw size or geometry. We demonstrated that a periodic array of cracks forms in the wake of the slider, with a critical spacing between the cracks. The critical spacing was calculated as a function of the loads applied to the indenter. We attempted to find conditions where neighboring cracks coalesce and form a wear particle, but found no such conditions. This suggests that, while fracture under contact loading can severely damage a solid, the rate of wear due to fracture is likely to be slow.

We also considered fracture under a cylinder which adhered perfectly bonded to the surface of the brittle solid. In this case, it was assumed that the cylinder was first pressed into the surface of the solid by a load P per unit length. Then, with P fixed, the cylinder was subjected to a steadily increasing tangential load Q. The tangential load gives rise to a singular distribution of traction at the trailing edge of the contact, so that a crack initiates spontaneously at a critical tangential load Q^{fract} given in (3.8). Thereafter, the crack path depends on the ratio of P/Q^{fract}. For small values of normal load, the crack follows a path which curves towards the free surface, so that a wear particle may be produced. For larger values of P/Q^{fract}, the crack tends to be driven to greater depths below the surface of the half-space. However, it always appears to curve back to the free surface eventually.

Finally, we determined the residual tensile strength of a solid damaged by contact loading. It was shown that contact fracture may reduce the strength of the solid by over an order of magnitude. We also calculated the magnitude of tensile residual stress required to cause catastrophic fracture under contact loading: again, the critical residual stress is a small fraction of the stress required to fracture the solid in the absence of contact loading.

ACKNOWLEDGEMENT

A.F.B. is grateful for support from the National Science Foundation through grant MSS-9210316.

REFERENCES

Auerbach, F. (1891) Measurement of hardness. *Ann. Phys. Chem.* **43,** 61–72.
Bethune, B. J. (1976) The surface cracking of glassy polymers under a sliding spherical indenter. *J. Mater. Sci.* **11,** 199–205.
Bower, A. F. and Johnson, K. L. (1989) The influence of strain hardening on cumulative plastic deformation in rolling and sliding contact. *J. Mech. Phys. Solids* **37**(4), 471–493.
Bryant, M. D., Miller, G. R. and Keer, L. M. (1984) Line contact between a rigid indenter and a damaged elastic body. *Q. J. Mech. Appl. Math.* **37**(3), 468–478.
Chaudhri, M. and Phillips, M. A. (1990) Quasi-static indentation cracking of thermally tempered soda-lime glass with spherical and Vickers indenters. *Phil. Mag.* **A62**(1), 1–27.
Chen, S. Y., Farris, T. N. and Chandrasekar, S. (1991) Sliding microindentation fracture of brittle materials. *S.T.L.E., Tribol. Trans.* **34**(2), 161–168.
Erdogan, F and Gupta, G. D. (1972) On the numerical integration of singular integral equations. *Q. Appl. Math.* **30,** 525–534.
Frank, F. C. and Lawn, B. R. (1967) On the theory of Hertzian fracture. *Proc. R. Soc. Lond.* **A299,** 291–306.
Gerasoulis, A. (1980) The use of piecewise quadratic polynomials for the solution of singular integral equations of Cauchy type. *Comp. Math. Appls* **8**(1), 15–22.
Green, A. E. and Zerna, W. (1968) *Theoretical Elasticity*. O.U.P., Reprinted by Dover Publications, 1992.
Johnson, K. L. (1985) *Contact Mechanics*. C.U.P., Cambridge.
Keer, L. M. and Bryant, M. D. (1983) A pitting model for rolling contact fatigue. *ASME J. Lub. Technol.* **105,** 198–205.
Keer, L. M. and Kuo, C. H. (1992) Cracking in a loaded brittle elastic half-space. *Int. J. Solids. Struct.* **29,** 1819–1826.
Keer, L. M. and Worden, R. E. (1990) A qualitative model to describe the microchipping wear mode in ceramic rollers. *Tribol. Trans.* **33,** 411–417.
Lawn, B. R. (1967) Partial cone crack formation in a brittle material loaded with a sliding spherical indenter. *Proc. R. Soc. Lond.* **A299,** 307–316.
Lawn, B. R. and Evans, A. G. (1977) A model for crack initiation in elastic/plastic indentation fields. *J. Mater. Sci.* **12,** 2195–2199.
Lawn, B. R., Evans, A. G. and Marshall, D. B. (1980) Elastic/plastic indentation damage in ceramics: the median/radial crack system. *J. Am. Ceram. Soc.* **63,** 574–581.
Lawn, B. R. and Marshall, D. B. (1978) Indentation fracture and strength degradation of ceramics. *Fracture Mechanics of ceramics*, Vol. 3 (ed. R. C. Bradt, D. P. H. Hasselman and F. F. Lange), pp. 205–229. Plenum Press, New York.
Marshall, D. B., Evans, A. G., Khuri Yakub, B. T., Tien, J. W. and King, G. S. (1983) The nature of machining damage in brittle materials. *Proc. R. Soc. Lond.* **A385,** 461–475.
Marshall, D. B. and Lawn, B. R. (1979) Residual stress effects in sharp contact cracking I: indentation fracture mechanics. *J. Mater. Sci.* **14,** 2001–2012.
Mouginot, R. and Maugis, D. (1985) Fracture indentation beneath flat and spherical punches. *J. Mater. Sci.* **20,** 4354–4376.
Nahrendran, V. M. and Cleary, M. P. (1984) Elastostatic interaction of multiple arbitrarily shaped cracks in plane inhomogeneous regions. *Engng Fract. Mech.* **19**(3), 481–506.

Roesler F. C. (1956) Brittle fractures near equilibrium. *Proc. Phys. Soc. Lond.* **B69,** 981–1012.

Swain, M. V.(1979) Microcracture at scratches in brittle solids. *Proc. R. Soc. Lond.* **A366,** 575–597.

Veldkamp, J. D. B., Hattu, N. and Snijders, V. A. C. (1978) Crack formation during scratching of brittle materials. *Fracture Mechanics of Ceramics*, Vol. 3 (ed. R. C. Bradt, D. P. H. Hasselman and F. F. Lange), pp. 273–301. Plenum Press, New York.